PHYSICAL REVIEW D **80,** 035019 (2009)

# Implications of the measurements of $B_s$–$\bar{B}_s$ mixing on supersymmetric models

P. Ko*
*School of Physics, KIAS, Seoul 130-722, Korea*

Jae-hyeon Park†
*INFN, Sezione di Padova, via F Marzolo 8, I-35131, Padova, Italy*
(Received 15 September 2008; published 25 August 2009)

We derive constraints on the mass insertion parameters from the recent measurements of $B_s$–$\bar{B}_s$ mixing, and discuss their implications on SUSY breaking mediation mechanisms and SUSY flavor models. Some SUSY flavor models are already excluded or disfavored by $B_s$–$\bar{B}_s$ mixing. We also discuss how to test the SM and SUSY models in the future experiments, by studying other $CP$ violating observables related to $b \to s$ transition, such as the time-dependent $CP$ asymmetry in $B_d \to \phi K_S$ and the direct $CP$ asymmetry in $B \to X_s \gamma$.

DOI: 10.1103/PhysRevD.80.035019 PACS numbers: 12.60.Jv, 11.30.Er, 13.25.Hw

## I. INTRODUCTION

Within the standard model (SM) with three families, there is a unique source of flavor and $CP$ violation in the quark sector, which is the renowned Cabbibo-Kobayashi-Maskawa (CKM) mixing matrix [1]. The CKM paradigm has long been tested in the $K$, $D$, and $B$ meson systems during the past decades. As of now, this picture has been well confirmed to describe basically all the data related with flavor and $CP$ violation in the quark sector, modulo some theoretical and experimental uncertainties. Experimental uncertainties will be decreased as more data are taken at $B$ factories, whereas theoretical uncertainties will be under better control when more results come from unquenched lattice QCD simulations on various nonperturbative parameters that are relevant to CKM analysis.

For many years, one of the important ingredients in the CKM phenomenology was still missing, namely $\Delta M_s$ from $B_s$–$\bar{B}_s$ mixing. Recently, however, $\Delta M_s$ was measured by both D0 and CDF Collaborations at the Tevatron [2,3]:

$$17\ \text{ps}^{-1} < \Delta M_s < 21\ \text{ps}^{-1} \quad \text{(D0)}, \tag{1.1}$$

$$\Delta M_s = (17.77 \pm 0.10 \pm 0.07)\ \text{ps}^{-1} \quad \text{(CDF)}. \tag{1.2}$$

One can use the measured value of $\Delta M_d/\Delta M_s$ to determine $|V_{td}/V_{ts}|$ within the SM [3]:

$$|V_{td}/V_{ts}| = 0.2060 \pm 0.0007(\Delta M_s)^{+0.0081}_{-0.0060}(\Delta M_d + \text{theor}). \tag{1.3}$$

This result is consistent with another independent determination of $|V_{td}/V_{ts}|$ from the Belle measurement of a radiative decay $b \to d\gamma$ [4]:

$$|V_{td}/V_{ts}| = 0.199^{+0.026}_{-0.025}(\text{exp})^{+0.018}_{-0.015}(\text{theor}). \tag{1.4}$$

Excellent agreement of these two independent measurements constitutes another firm test of the CKM paradigm for flavor and $CP$ violation in the SM [5,6], and puts strong constraints on various new physics scenarios. There are model independent analyses of $\Delta M_s$ measurements on general new physics [7,8], as well as analyses within supersymmetric (SUSY) models [9,10] and others [11]. Because of these data on $\Delta M_s$, the CKM paradigm is more constrained than before, and there may be even a slight hint for new physics beyond the SM (see Ref. [8], for example).

Within the SM, $B_s$–$\bar{B}_s$ mixing is dominated by $t$-$W$ loop, and the $B_s$–$\bar{B}_s$ mixing phase is suppressed by $\lambda^2$ [12]. Because of its small theoretical uncertainty, observation of a nonzero discrepancy in the phase of $B_s$–$\bar{B}_s$ mixing would be an unambiguous signal of new physics beyond the SM in $b \to s$ transition [13]. Such new physics effects, if any, may appear in other observables in the $B_{(d,s)}$ meson systems, e.g., $B_d \to \phi K_S$ or $B \to X_s \gamma$.

The two collaborations also reported results on the phase of $B_s$–$\bar{B}_s$ mixing from the time-dependent $CP$ asymmetry in $B_s \to J/\psi\phi$. The results are [14,15]

$$\phi_s = -0.57^{+0.24}_{-0.30}(\text{stat})^{+0.07}_{-0.02}(\text{syst}) \quad \text{(D0)}, \tag{1.5}$$

$$\phi_s \in [-1.36, -0.24] \cup [-2.90, -1.78] \quad \text{(CDF)}, \tag{1.6}$$

at 68% C.L. These measurements give a strong constraint on the new physics contributions to $B_s$–$\bar{B}_s$ mixing, both the modulus and the phase of the mixing. In general SUSY models, this will constrain the 23 mixing, $(\delta^d_{23})_{AB}$ with $A, B = L$ or $R$.

In this paper, we update our previous studies on $b \to s$ transitions within the general SUSY models [16,17] using the new data on $B_s$ mixing from D0 and CDF, and discuss their implications for SUSY models. In Sec. II, we describe the general SUSY models with gluino-mediated flavor/$CP$ violation in brief, and how to proceed and analyze the SUSY models. Compared with the previous studies, we consider the $\tan\beta$ dependent constraint carefully including the double mass insertions, which can be prominent in

*pko@kias.re.kr
†jae-hyeon.park@pd.infn.it

 

$B \to X_s\gamma$ for large tan$\beta$. In Sec. III, we present the constraints on the mass insertion parameters for several different scenarios: the $LL$ or the $RR$ dominance case, and $LL = \pm RR$ cases. In Sec. IV, we discuss implications of the newly derived bounds on the mass insertion parameters on SUSY models. Most SUSY models with universal soft scalar masses at some high energy scale or many SUSY models with flavor symmetry groups are still consistent with our new constraints. But some SUSY flavor models based on flavor symmetries and alignment of quark and squark mass matrices are shown to be in conflict with our constraints, and thus excluded or disfavored, depending on tan$\beta$. In Sec. V, we summarize our results and discuss the prospects in the future directions in theory and experiments which should be taken in order to test the CKM paradigm and see by any chance some new physics effects lurking in $b \to s$ transitions.

## II. MODELS AND ANALYSIS PROCEDURES

### A. Gluino-mediated flavor violation and mass insertion approximation

The minimal supersymmetric standard model (MSSM) has many nice motivations such as resolution of the fine-tuning problem of the Higgs mass parameter, gauge coupling unification, and cold dark matter [18]. But SUSY, if it exists, must be broken, and the SUSY breaking effect is described phenomenologically by more than 100 new parameters in the so-called soft SUSY breaking Lagrangian. These soft SUSY breaking parameters generically violate both flavor and $CP$. If these parameters take generic values, one ends up with excessive flavor and $CP$ violations which are already inconsistent with such low energy data as $K^0$–$\bar{K}^0$ mixing, $\epsilon_K$, $B \to X_s\gamma$, and electron/neutron electric dipole moments (EDMs). Therefore, there must be some mechanism which controls the structures of flavor changing neutral currents (FCNCs) and $CP$ in the soft SUSY breaking terms, if weak scale SUSY has anything to do with Nature. This may be achieved by means of the SUSY breaking mediation mechanism which is flavor blind, and/or some flavor symmetry controlling both Yukawa couplings and sfermion mass matrices in flavor space. In a different point of view, we could get a clue to these SUSY breaking mediation mechanisms by studying FCNC and $CP$ in supersymmetric models.

In SUSY models, there are new contributions to $B_s$–$\bar{B}_s$ mixing from $H^-$–$t$, $\chi^-$–$\tilde{U}_i$, and $\tilde{D}_i$–$\tilde{g}(\tilde{\chi}^0)$ in addition to the SM $t$-$W$ loop. In generic SUSY models, the squark-gluino-loop contribution is parametrically larger than other contributions, since it is a strong interaction. In this work, we assume that the dominant SUSY contribution to $B_s$ mixing comes from down-squark-gluino-loop diagrams. This assumption simplifies the numerical analysis considerably. Including effects from other SUSY particles is straightforward, and similar analysis could be done. A similar analysis for the $b \to d$ transition has been performed within the mass insertion approximation [19], using $B_d$–$\bar{B}_d$ mixing, the $CP$ asymmetry in semileptonic (SL) $B$ meson decay $A_{\rm SL}^d$, and $CP$ violation in $B \to X_d\gamma$ under the same assumptions.

Mass insertion approximation is a useful tool to present flavor and $CP$ violations in the sfermion sector in generic SUSY models [20]. The parameter $(\delta_{ij}^q)_{AB}$ represents the dimensionless transition strength from $\tilde{q}_{jB}$ to $\tilde{q}_{iA}$ in the basis where the fermion Yukawa couplings are diagonal (super-CKM basis), where $q = u, d$ indicates whether the squarks are of up-type or down-type, $i, j = 1, 2, 3$ are generation indices, and $A, B = L, R$ are chiralities of superpartners of the squarks.[1] If $(\delta_{ij}^d)_{AB} \sim O(1)$, there are excessive FCNC and $CP$ violations with strong interaction couplings, which are clearly excluded by the data. Therefore $\delta$'s should be small, $\lesssim 10^{-1}$–$10^{-3}$ with upper bounds depending on $(i, j, A, B)$, which is so called the SUSY FCNC/$CP$ problem.

Current global analysis of the CKM matrix elements indicates that any new physics around TeV scale should be flavor/$CP$ blind to a very good approximation. Therefore it would be nice if we can set $\delta = 0$. However, even if we set $\delta$'s to zero by hand at one energy scale (presumably at high energy scale), nonzero $\delta$'s are regenerated at electroweak scale due to the renormalization group (RG) evolution, and we cannot make $\delta$'s vanish at all scales. It is most likely that $\delta$'s are nonvanishing at electroweak scale. Then, the relevant questions are how large or small $\delta$ parameters are in a given SUSY breaking scenario, and what are the observable consequences of nonzero $\delta$'s in flavor and $CP$ violation beyond the effects derived from CKM matrix elements. These issues will be addressed in the subsequent sections.

Since flavor physics and $CP$ violation such as $B \to X_s\gamma$, $B_s \to \mu^+\mu^-$, $\epsilon_K$ within SUSY models depend strongly on the soft SUSY breaking sector which is not well understood yet, it is important not to make an *ad hoc* assumption on the soft terms. For example, the usual assumption in the mSUGRA scenario is not well motivated theoretically, although it seems acceptable phenomenologically since it solves the SUSY flavor and $CP$ problem. However, such assumptions are made for the sake of simplicity in studying flavor physics, dark matter, and collider physics signatures within SUSY context. Sometimes, it gives wrong intuitions, some examples of which can be found in Ref. [21].

In the following, we at first consider $\delta$'s as free parameters at the electroweak scale, and derive phenomenological constraints on these parameters, including $B \to X_s\gamma$ and the newly measured $B_s$–$\bar{B}_s$ mixing. Then we estimate the $\delta$'s in various SUSY breaking scenarios, and investigate which models pass the phenomenological constraints on $\delta$ parameters. We assume $\delta$'s vanish at some scale (messen-

[1] A quantitative definition of the $\delta$ parameters will be given below.

ger scale), where soft SUSY breaking terms are generated, and study the size of the $\delta$'s that are generated by RG evolutions down to the electroweak scale. Alternatively, we consider SUSY flavor models where $\delta$'s are controlled by some flavor symmetry group that acts on the flavor indices of quarks and their superpartners.

In terms of mass insertion parameters $(\delta^d_{ij})_{AB}$, the down-type squark mass matrix of second and third families can be written as

$$M^2_{\tilde{d}} = \begin{pmatrix} \tilde{m}^2_L + \tilde{m}^2 & \tilde{m}^2(\delta^d_{23})_{LL} & m_s(A_s - \mu\tan\beta) & \tilde{m}^2(\delta^d_{23})_{LR} \\ \tilde{m}^2(\delta^d_{23})^*_{LL} & \tilde{m}^2_L + \tilde{m}^2 & \tilde{m}^2(\delta^d_{23})^*_{RL} & m_b(A_b - \mu\tan\beta) \\ m_s(A_s - \mu\tan\beta) & \tilde{m}^2(\delta^d_{23})_{RL} & \tilde{m}^2_R + \tilde{m}^2 & \tilde{m}^2(\delta^d_{23})_{RR} \\ \tilde{m}^2(\delta^d_{23})^*_{LR} & m_b(A_b - \mu\tan\beta) & \tilde{m}^2(\delta^d_{23})^*_{RR} & \tilde{m}^2_R + \tilde{m}^2 \end{pmatrix}, \tag{2.1}$$

where $\tilde{m}^2$ is the universal part of soft SUSY breaking scalar mass squared, and

$$\begin{aligned} \tilde{m}^2_L &= -\tfrac{1}{6}\cos 2\beta(m^2_Z + 2m^2_W), \\ \tilde{m}^2_R &= -\tfrac{1}{3}\cos 2\beta(m^2_Z - m^2_W) \end{aligned} \tag{2.2}$$

are $D$-term contributions. We neglect $m^2_d$ terms. We assume that $A$ terms are negligible, and the $\mu$ parameter is real. Relaxing the former assumption is straightforward, and would not change the results significantly. The latter assumption is made to satisfy EDM constraints. By using mass insertion parameters, we have implicitly specified the basis of squark flavors, i.e. the above matrix is in the super CKM basis. The unitary matrix $U$ diagonalizing the mass matrix is divided into two parts, $\Gamma_L$ and $\Gamma_R$, according to the quark chirality to which they are associated, as

$$M^2_{\tilde{d}} = U^\dagger M^{2(\mathrm{diag})}_{\tilde{d}} U, \qquad \Gamma^{Ij}_L \equiv U^I{}_j, \qquad \Gamma^{Ij}_R \equiv -U^I{}_{j+3}, \tag{2.3}$$

where $M^{2(\mathrm{diag})}_{\tilde{d}}$ is a diagonal matrix with positive elements, $I = 1, \ldots, 6$ is the squark mass eigenstate index, and $j = 1, 2, 3$ is the quark mass eigenstate index. Note that we absorb the relative minus sign between quark-squark-gluino vertices of opposite chiralities into that in the definition of $\Gamma^{Ij}_R$. We give a name $r_I$ to the ratio of a squark squared mass eigenvalue to the gluino mass squared,

$$r_I \equiv \frac{[M^{2(\mathrm{diag})}_{\tilde{d}}]_{II}}{m^2_{\tilde{g}}}, \tag{2.4}$$

which we will use to express Wilson coefficients later on.

### B. $\Delta B = 2$ effective Hamiltonian

For $B_s$–$\bar{B}_s$ mixing, we use the $\Delta B = 2 (= -\Delta S)$ effective Hamiltonian. We first integrate out SUSY particles and derive effective Hamiltonian at sparticle mass scale. Then we use the renormalization group running formula from the sparticle mass scale to $m_b$ scale presented in [22]. The resulting effective Hamiltonian can be written as

$$\mathcal{H}^{\Delta B=2}_{\mathrm{eff}} = \sum_{i=1}^{5} \mathcal{C}_i Q_i + \sum_{i=1}^{3} \tilde{\mathcal{C}}_i \tilde{Q}_i + \mathrm{H.c.}, \tag{2.5}$$

where we choose the operator basis as follows:

$$\begin{aligned} Q_1 &= \bar{s}^\alpha_L \gamma_\mu b^\alpha_L \bar{s}^\beta_L \gamma^\mu b^\beta_L, \qquad Q_2 = \bar{s}^\alpha_R b^\alpha_L \bar{s}^\beta_R b^\beta_L, \\ Q_3 &= \bar{s}^\alpha_R b^\beta_L \bar{s}^\beta_R b^\alpha_L, \qquad Q_4 = \bar{s}^\alpha_R b^\alpha_L \bar{s}^\beta_L b^\beta_R, \\ Q_5 &= \bar{s}^\alpha_R b^\beta_L \bar{s}^\beta_L b^\alpha_R, \end{aligned} \tag{2.6}$$

where $\alpha$ and $\beta$ are color indices. The Wilson coefficients $\mathcal{C}_i$'s associated with the operators $Q_i$'s are given by

$$\begin{aligned} \mathcal{C}_1 &= \frac{\alpha^2_s}{216 m^2_{\tilde{g}}} \sum_{IJ} \Gamma^{I2*}_L \Gamma^{I3}_L \Gamma^{J2*}_L \Gamma^{J3}_L (-24 B_2(r_I, r_J) - 264 B_1(r_I, r_J)), \\ \mathcal{C}_2 &= \frac{\alpha^2_s}{216 m^2_{\tilde{g}}} \sum_{IJ} \Gamma^{I2*}_R \Gamma^{I3}_L \Gamma^{J2*}_R \Gamma^{J3}_L (-204 B_2(r_I, r_J)), \\ \mathcal{C}_3 &= \frac{\alpha^2_s}{216 m^2_{\tilde{g}}} \sum_{IJ} \Gamma^{I2*}_R \Gamma^{I3}_L \Gamma^{J2*}_R \Gamma^{J3}_L (36 B_2(r_I, r_J)), \\ \mathcal{C}_4 &= \frac{\alpha^2_s}{216 m^2_{\tilde{g}}} \left[ \sum_{IJ} \Gamma^{I2*}_R \Gamma^{I3}_R \Gamma^{J2*}_L \Gamma^{J3}_L (-504 B_2(r_I, r_J) + 288 B_1(r_I, r_J)) + \sum_{IJ} \Gamma^{I2*}_L \Gamma^{I3}_R \Gamma^{J2*}_R \Gamma^{J3}_L (528 B_1(r_I, r_J)) \right], \\ \mathcal{C}_5 &= \frac{\alpha^2_s}{216 m^2_{\tilde{g}}} \left[ \sum_{IJ} \Gamma^{I2*}_R \Gamma^{I3}_R \Gamma^{J2*}_L \Gamma^{J3}_L (-24 B_2(r_I, r_J) - 480 B_1(r_I, r_J)) + \sum_{IJ} \Gamma^{I2*}_L \Gamma^{I3}_R \Gamma^{J2*}_R \Gamma^{J3}_L (720 B_1(r_I, r_J)) \right], \end{aligned} \tag{2.7}$$

where we use the notation

$$B_i(r_I, r_J) = \frac{B_i(r_I) - B_i(r_J)}{r_I - r_J}, \qquad i = 1, 2, \tag{2.8}$$

with [23]

$$\begin{aligned} B_1(r) &= -\frac{r^2 \ln r}{4(1-r)^2} - \frac{1}{4(1-r)}, \\ B_2(r) &= -\frac{r \ln r}{(1-r)^2} - \frac{1}{1-r}. \end{aligned} \tag{2.9}$$

One can get $\tilde{O}_i$ and $\tilde{C}_i$ for $i = 1, 2, 3$ by exchanging $L \leftrightarrow R$.

For the matrix elements of the above operators and the numerical values of $B_{1,\ldots,5}(\mu)$ and $f_{B_d}$, we use the values given in Ref. [22]. We use the following ratio:

$$\frac{f_{B_s}\sqrt{B_{B_s}}}{f_{B_d}\sqrt{B_{B_d}}} = 1.21, \tag{2.10}$$

given in Ref. [24].

### C. $\Delta B = 1$ effective Hamiltonian

Nonleptonic charmless and radiative $B_{d(s)}$ decays are described by the following $\Delta B = 1$ effective Hamiltonian. We use the same normalization of operator basis as in Ref. [17]. The RG running of gluino-loop contributions from $m_W$ scale to $m_b$ scale is performed in the way presented in [25], i.e., the $\alpha_s^n$ factor from the quark-squark-gluino vertices is included in an operator rather than the corresponding Wilson coefficient, and the dimension-five and dimension-six versions of the (chromo) magnetic operators are treated separately. Then the $\Delta B = 1$ effective Hamiltonian encoding the gluino-squark loop contribution can be written as

$$\begin{aligned} \mathcal{H}_{\text{eff}}^{\Delta B=1} = \frac{G_F}{\sqrt{2}} \sum_{p=u,c} \lambda_p \Bigg[ & \sum_{i=3}^{6} (C_i O_i + \tilde{C}_i \tilde{O}_i) \\ & + \sum_{i=7\gamma,8g} (C_{ib} O_{ib} + C_{i\tilde{g}} O_{i\tilde{g}} + \tilde{C}_{ib} \tilde{O}_{ib} \\ & + \tilde{C}_{i\tilde{g}} \tilde{O}_{i\tilde{g}}) \Bigg] + \text{H.c.}, \end{aligned} \tag{2.11}$$

where $\lambda_p = V_{ps}^* V_{pb}$. The operator basis is chosen as follows:

$$\begin{aligned} O_3 &= \alpha_s^2 (\bar{s} b)_{V-A} \sum_q (\bar{q} q)_{V-A}, \\ O_4 &= \alpha_s^2 (\bar{s}_\alpha b_\beta)_{V-A} \sum_q (\bar{q}_\beta q_\alpha)_{V-A}, \\ O_5 &= \alpha_s^2 (\bar{s} b)_{V-A} \sum_q (\bar{q} q)_{V+A}, \\ O_6 &= \alpha_s^2 (\bar{s}_\alpha b_\beta)_{V-A} \sum_q (\bar{q}_\beta q_\alpha)_{V+A}, \\ O_{7\gamma b} &= -\frac{\alpha_s e}{8\pi^2} m_b \bar{s} \sigma_{\mu\nu} (1+\gamma_5) F^{\mu\nu} b, \\ O_{8g b} &= -\frac{\alpha_s g_s}{8\pi^2} m_b \bar{s} \sigma_{\mu\nu} (1+\gamma_5) G^{\mu\nu} b, \\ O_{7\gamma\tilde{g}} &= -\frac{\alpha_s e}{8\pi^2} \bar{s} \sigma_{\mu\nu} (1+\gamma_5) F^{\mu\nu} b, \\ O_{8g\tilde{g}} &= -\frac{\alpha_s g_s}{8\pi^2} \bar{s} \sigma_{\mu\nu} (1+\gamma_5) G^{\mu\nu} b. \end{aligned} \tag{2.12}$$

The corresponding Wilson coefficients $C_i$'s are given by

$$\begin{aligned} C_3 &= -\frac{1}{2\sqrt{2} G_F m_{\tilde{g}}^2 \lambda_t} \Bigg[ \sum_I \Gamma_L^{I2*} \Gamma_L^{I3} \left( -\frac{1}{18} C_1(r_I) + \frac{1}{2} C_2(r_I) \right) + \sum_{IJ} \Gamma_L^{I2*} \Gamma_L^{I3} \Gamma_L^{J2*} \Gamma_L^{J2} \left( -\frac{1}{9} B_1(r_I, r_J) - \frac{5}{9} B_2(r_I, r_J) \right) \Bigg], \\ C_4 &= -\frac{1}{2\sqrt{2} G_F m_{\tilde{g}}^2 \lambda_t} \Bigg[ \sum_I \Gamma_L^{I2*} \Gamma_L^{I3} \left( \frac{1}{6} C_1(r_I) - \frac{3}{2} C_2(r_I) \right) + \sum_{IJ} \Gamma_L^{I2*} \Gamma_L^{I3} \Gamma_L^{J2*} \Gamma_L^{J2} \left( -\frac{7}{3} B_1(r_I, r_J) + \frac{1}{3} B_2(r_I, r_J) \right) \Bigg], \\ C_5 &= -\frac{1}{2\sqrt{2} G_F m_{\tilde{g}}^2 \lambda_t} \Bigg[ \sum_I \Gamma_L^{I2*} \Gamma_L^{I3} \left( -\frac{1}{18} C_1(r_I) + \frac{1}{2} C_2(r_I) \right) + \sum_{IJ} \Gamma_L^{I2*} \Gamma_L^{I3} \Gamma_R^{J2*} \Gamma_R^{J2} \left( \frac{10}{9} B_1(r_I, r_J) + \frac{1}{18} B_2(r_I, r_J) \right) \Bigg], \\ C_6 &= -\frac{1}{2\sqrt{2} G_F m_{\tilde{g}}^2 \lambda_t} \Bigg[ \sum_I \Gamma_L^{I2*} \Gamma_L^{I3} \left( \frac{1}{6} C_1(r_I) - \frac{3}{2} C_2(r_I) \right) + \sum_{IJ} \Gamma_L^{I2*} \Gamma_L^{I3} \Gamma_R^{J2*} \Gamma_R^{J2} \left( -\frac{2}{3} B_1(r_I, r_J) + \frac{7}{6} B_2(r_I, r_J) \right) \Bigg], \\ C_{7\gamma b} &= -\frac{\pi}{\sqrt{2} G_F m_{\tilde{g}}^2 \lambda_t} \sum_I \Gamma_L^{I2*} \Gamma_L^{I3} \left( -\frac{4}{9} D_1(r_I) \right), \\ C_{7\gamma\tilde{g}} &= -\frac{\pi}{\sqrt{2} G_F m_{\tilde{g}}^2 \lambda_t} \sum_I \Gamma_L^{I2*} \Gamma_R^{I3} \left( -\frac{4}{9} D_2(r_I) \right), \\ C_{8\gamma b} &= -\frac{\pi}{\sqrt{2} G_F m_{\tilde{g}}^2 \lambda_t} \sum_I \Gamma_L^{I2*} \Gamma_L^{I3} \left( -\frac{1}{6} D_1(r_I) + \frac{3}{2} D_3(r_I) \right), \\ C_{8\gamma\tilde{g}} &= -\frac{\pi}{\sqrt{2} G_F m_{\tilde{g}}^2 \lambda_t} \sum_I \Gamma_L^{I2*} \Gamma_R^{I3} \left( -\frac{1}{6} D_2(r_I) + \frac{3}{2} D_4(r_I) \right). \end{aligned} \tag{2.13}$$

One can get $\tilde{O}_i$ and $\tilde{C}_i$ for $i = 3, \ldots, 6, 7\gamma, 8g$ by exchanging $L \leftrightarrow R$. The loop functions are given by Eqs. (2.8) and (2.9), and [23]:

$$C_1(r) = \frac{2r^3 - 9r^2 + 18r - 11 - 6\ln r}{36(1-r)^4},$$
$$C_2(r) = \frac{-16r^3 + 45r^2 - 36r + 7 + 6r^2(2r-3)\ln r}{36(1-r)^4},$$
$$D_1(r) = \frac{-r^3 + 6r^2 - 3r - 2 - 6r\ln r}{6(1-r)^4},$$
$$D_2(r) = \frac{-r^2 + 1 + 2r\ln r}{(r-1)^3}, \tag{2.14}$$
$$D_3(r) = \frac{2r^3 + 3r^2 - 6r + 1 - 6r^2\ln r}{6(1-r)^4},$$
$$D_4(r) = \frac{-3r^2 + 4r - 1 + 2r^2\ln r}{(r-1)^3}.$$

### D. New elements in this analysis

SUSY effects in $B_s$ mixing before the CDF/D0 measurements of $\Delta M_s$ have been discussed comprehensively in the literature [16,17,26]. This work is an update of our previous works [16,17], including a few new elements and improvements in the analysis:

(i) We include the $\tan\beta$ dependent double mass insertion more carefully. As a result, the $B \to X_s\gamma$ branching ratio constrains not only the $LR$ and $RL$ insertions, but also the $LL$ and $RR$ insertions, because of the induced $LR$ and $RL$ mass insertions. Double mass insertion contribution to $B \to X_s\gamma$ has long been known [27]. The potential importance of the double mass insertion was discussed in Ref. [28] in the context of supersymmetric contributions to $\mathrm{Re}(\epsilon'/\epsilon)$ using the $s \to dg$ operator, and similarly in Refs. [29–31] regarding $b \to s$ transitions. We discuss more on this in the next subsection in the context of $b \to s\gamma$ and $b \to sg$. Because of this improvement, we get stronger constraints on the pure $LL$ or $RR$ insertion, compared with our previous study [17], especially for large $\tan\beta$. (However, see also [32].)

(ii) We also consider the simultaneous presence of the $LL$ and $RR$ insertions, motivated by some SUSY flavor models which predict $LL \approx RR$. We find that the $\Delta M_s$ measurement puts a stringent constraint on such cases, independent of $\tan\beta$ [27,30,31]. Our analysis shows that some SUSY flavor models are already excluded by (or marginally compatible with) the $\Delta M_s$ measurement of the CDF/D0. Partly for simplicity, we consider only two cases where the two insertions are assumed to be correlated by $(\delta^d_{23})_{LL} = \pm(\delta^d_{23})_{RR}$. Regarding their phases, however, there are good reasons to restrict their difference around 0 or $\pi$. Sizable $LL$ and $RR$ mass insertions with uncorrelated phases are likely to give an excessive contribution to the neutron EDM [33]. For instance, if $\mu = 500$ GeV and the sizes of the two insertions are both around 0.05 [see Figs. 6–8 and 9(a)], then the neutron EDM limits their relative phase within $\lesssim 0.8/\tan\beta$ around 0 or $\pi$.

(iii) We include the D0/CDF data on the phase of $B_s$ mixing deduced from the dilepton charge asymmetry and $B_s \to J/\psi\phi$ [14,15,34]. In particular, we discuss consequences of the present tendency of the data favoring a negative $O(1)$ value of $\phi_s$ [35].

(iv) We present the time-dependent $CP$ asymmetry in $B^0 \to K^{*0}\gamma$, in cases with right-handed $b \leftrightarrow s$ currents such as from the $RR$ insertion. See Ref. [36] for more details on this observable.

(v) In this paper, we consider only the $LL$ and $RR$ insertions, and do not consider $LR$ or $RL$ insertion, because the new data on $\Delta M_s$ does not affect the analysis in Refs. [16,17] on $LR$ or $RL$ insertion. In that article, we have found that the $B \to X_s\gamma$ constraint on these chirality-flipping insertions is so strong that they cannot give an appreciable modification to $\Delta M_s$ or $\phi_s$ [17,26].

### E. Double mass insertion

If the $LL$ or $RR$ insertion is sizable and $\mu\tan\beta$ is large, an effective $LR$ or $RL$ insertion can be induced due to the double mass insertion mechanism we discussed in the previous subsection and in Refs. [27–29]. Then we can expect that $B \to X_s\gamma$ could give a strong constraint on the $LL$ or $RR$ insertion through this effective $LR$ or $RL$ insertion. The relevant Feynman diagram is shown in Fig. 1. The induced $LR$ or $RL$ from double mass insertion can be written schematically as

$$(\delta^d_{LR})^{\mathrm{ind}}_{23} = (\delta^d_{LL})_{23} \times \frac{m_b(A_b - \mu\tan\beta)}{\tilde{m}^2}. \tag{2.15}$$

Therefore, we have

$$(\delta^d_{LL,RR})_{23} \sim 10^{-2} \to (\delta^d_{LR,RL})^{\mathrm{ind}}_{23} \sim 10^{-2},$$

if $\mu\tan\beta \sim 30$ TeV. This can be expected if $\tan\beta$ is large $\sim$40. For larger $LL$, $RR$ mixing, even smaller $\mu\tan\beta$ would suffice to induce the $LR$, $RL$ mass insertions of a size $10^{-2}$–$10^{-3}$. Since $\delta_{LL,RR}$'s in SUSY flavor models are

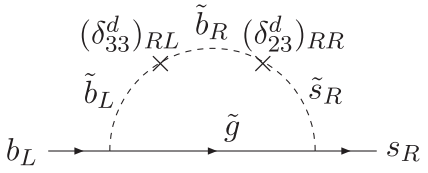


FIG. 1. Gluino-squark loop graph with double mass insertion for $B \to X_s\gamma$.

generically complex, the induced $(\delta^d_{LR})^{\rm ind}_{23}$ could carry a new $CP$ violating phase even if the trilinear coupling $A_b$ and $\mu$ parameters are real. In such a case, there could be strong correlations among various $CP$ violating observables. The effects of these induced $LR$ or $RL$ mixings appear in the deviations in $S^{\phi K}_{CP}$, $A^{b\to s\gamma}_{CP}$, or $S^{K^*\gamma}_{CP}$ from their SM predictions.

It is important to remember that the effect of the induced $LR$ insertion is different from that of the single $LR$ insertion, since they involve different numbers of squark propagators in the relevant Feynman diagrams, and thus yielding different loop functions when one evaluates the Feynman diagrams.

### F. Numerical analysis

In the following discussions and numerical analysis, we fix the SUSY parameters as follows once and for all:

$$m_{\tilde q} = m_{\tilde g} = \mu = 500\ \text{GeV}, \qquad \tan\beta = 3 \text{ and } 10,$$

taking the mass insertion parameters $(\delta^d_{23})_{AB}$'s as free complex parameters. We do not consider very high $\tan\beta \gtrsim 30$ at which the double Higgs penguin contribution may be important [10,37]. Since we do not include the chargino contributions in this work, the sign of $\mu$ could be either positive or negative. However, we choose a positive $\mu$, since it is preferred by the muon $g-2$ when we include the chargino or the neutralino contributions. The plots for a negative $\mu$ are similar to those for a positive $\mu$. If the supersymmetric contribution to an observable is dominated by double mass insertion, the region allowed by it is almost reflected around zero. The small difference arises from interference between single and double insertions. Such observables include $B(B\to X_s\gamma)$, $A^{b\to s\gamma}_{CP}$, $S^{\phi K}_{CP}$, and $S^{K^*\gamma}_{CP}$. Therefore, the compatibility of each case with these observables discussed later largely remains the same even if we take the negative sign of $\mu$. When we scan over the complex parameter $(\delta^d_{23})_{AB}$'s, we impose the following constraints and show the excluded regions:

(i) The smallest squared mass eigenvalue in $M^2_{\tilde d}$ is required to be greater than $(100\ \text{GeV})^2$. The region incompatible with this requirement is denoted by gray hatched regions.

(ii) The branching ratio of $B\to X_s\gamma$ is required to be within its $2\sigma$ range [6],

$$3.0\times10^{-4} < B(B\to X_s\gamma) < 4.1\times10^{-4}. \quad (2.16)$$

The region incompatible with this requirement is denoted by hatched regions.

(iii) The region allowed by $12.4\ \text{ps}^{-1} < \Delta M_s < 23.1\ \text{ps}^{-1}$ is denoted by cyan regions. We allow for up to 30% of the deviation of $\Delta M_s$ from the CDF central value [3], considering uncertainties in lattice QCD calculation and the CKM matrix elements (see e.g. [38] and references therein).

(iv) The region allowed by both the $\Delta M_s$ constraint and $\phi_s \in [-1.10, -0.36]\cup[-2.77, -2.07]$ [35], where $\phi_s$ is $\arg(M_{12})$, is denoted by blue regions. We take the latest 95% probability range of $\phi_s$. We adopt the sign of $\phi_s$ used in Refs. [39,40].

(v) Then we predict the time-dependent $CP$ asymmetry $(S^{\phi K}_{CP})$ in $B_d\to\phi K_S$, that $(S^{K^*\gamma}_{CP})$ in $B^0\to K^{*0}\gamma$, and the direct $CP$ asymmetry $(A^{b\to s\gamma}_{CP})$ in $B\to X_s\gamma$.

(vi) A black square denotes the SM prediction for each observable.

(vii) We show the region corresponding to the $2\sigma$ range of $S^{\phi K}_{CP}$ in the plots for the allowed regions in the $(\text{Re}\delta, \text{Im}\delta)$ plane, using the current average $S^{\phi K}_{CP} = 0.39 \pm 0.18$ [6]. For this, we take into account the uncertainty in the prediction of $S^{\phi K}_{CP}$ coming from the annihilation contribution in QCD factorization [41] in the same way as in Sec. VI E of Ref. [17]. That is, the prediction of $S^{\phi K}_{CP}$ from a single point of $\delta$ forms an interval. We exclude the point of $\delta$ if the interval is mutually exclusive with the $2\sigma$ range from experiments. We use this interval in a correlation plot as well.

## III. SUSY EFFECTS IN $b\to s$ AFTER THE CDF/D0 MEASUREMENTS OF $\Delta M_s$

### A. $LL$ insertion case

Let us first consider the $LL$ insertion (or $LL$ dominance) case with $\tan\beta = 3$. In the previous study [16,17], we ignored the double mass insertion so that the constraint on the $LL$ insertion was not very strong. In this work, we include the induced $LR$ insertion which is dependent on $\tan\beta$. Therefore, the $B\to X_s\gamma$ branching ratio puts a strong constraint, even before we impose the $\Delta M_s$ measurements. Only the unhatched region is consistent with the $B\to X_s\gamma$ constraint in Fig. 2(a). A substantial part of $(\delta^d_{23})_{LL}$ is already excluded by $B\to X_s\gamma$. After imposing the CDF/D0 data on $\Delta M_s$ and $\phi_s$, only the blue region remains allowed. It is outstanding that the SM point lies outside the blue region indicating that the current $\phi_s$ data, with the aid of $\Delta M_s$, is pointing to a new source of flavor/$CP$ violation. Moreover, the size of insertion needed to fit the $B_s$ mixing data is of $O(1)$. This large insertion inevitably disturbs $B\to X_s\gamma$ through the double mass insertion mechanism involving the $\mu\tan\beta$ term. Indeed, one finds that most of the blue region is ruled out by the branching ratio of $B\to X_s\gamma$. Note that $B\to X_s\gamma$ is this stringent already with $\tan\beta$ as low as 3 and that it grows tighter as $\tan\beta$ increases as we will see shortly. Still, there are corners compatible with $B\to X_s\gamma$ as well as $B_s$–$\bar B_s$ mixing, which is evident from Fig. 2(b). The plot also shows that one of the two $\phi_s$ solutions is excluded by $B\to X_s\gamma$. The double insertion leads to sizable changes in $S^{\phi K}_{CP}$ or $A^{b\to s\gamma}_{CP}$ as well. Figure 2(c) shows that $B\to X_s\gamma$ and

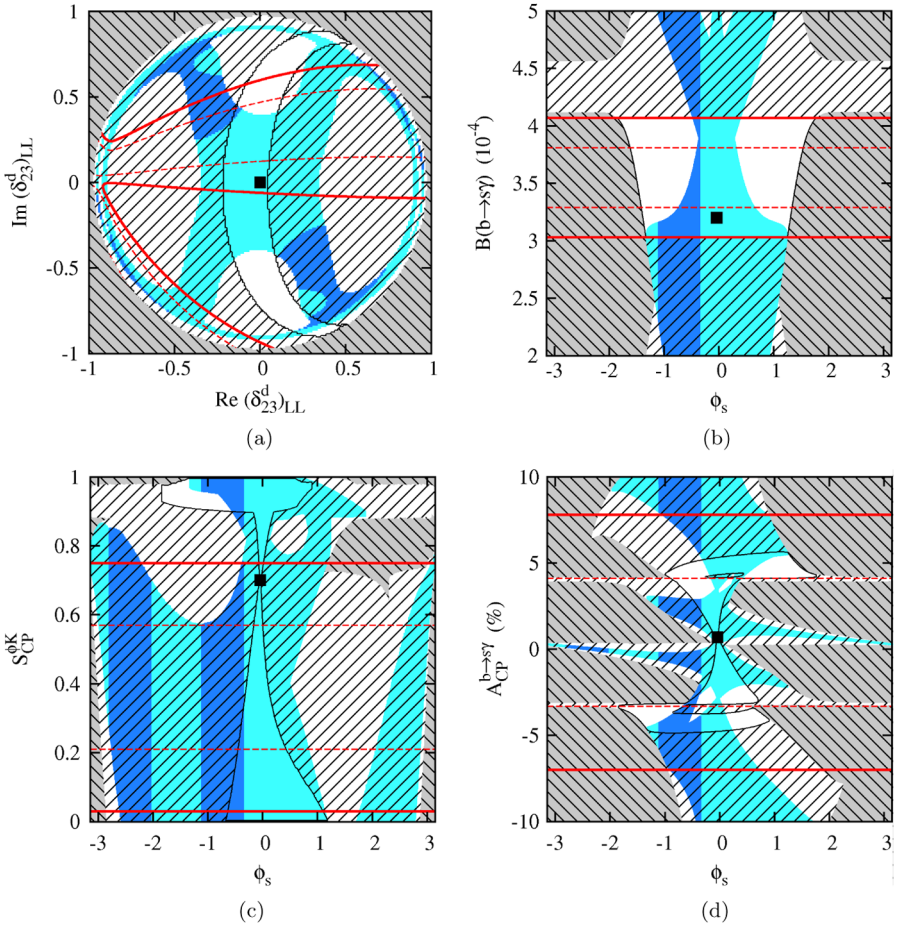


FIG. 2 (color online). The $LL$ insertion case with $\tan\beta = 3$. Allowed regions on (a) $[\mathrm{Re}(\delta^d_{23})_{LL}, \mathrm{Im}(\delta^d_{23})_{LL}]$, and correlation between $\phi_s$ and each of (b) $B(B \to X_s\gamma)$, (c) $S^{\phi K}_{CP}$, and (d) $A^{b\to s\gamma}_{CP}$. The hatched gray region leads to the lightest squark mass $<100$ GeV. The hatched region is excluded by the $B \to X_s\gamma$ constraint. The gray (cyan online) region is allowed by $\Delta M_s$. The dark gray (blue online) region is allowed both by $\Delta M_s$ and $\phi_s$. The black square is the SM point. In (a), bands bounded by red dashed and solid curves correspond to $1\sigma$ and $2\sigma$ ranges of $S_{\phi K}$, respectively. In the rest of the figures, red dashed and solid lines mark $1\sigma$ and $2\sigma$ ranges of each observable, respectively.

$B_s$–$\bar{B}_s$ mixing, together, disfavor $S^{\phi K}_{CP}$ around its SM value, although it is still permitted to fall within its $2\sigma$ range. The same set of constraints results in $A^{b\to s\gamma}_{CP}$ of $\pm$ a few percent, as displayed in Fig. 2(d), which can be discriminated from the SM prediction at a super $B$ factory.

For $\tan\beta = 10$, the double mass insertion becomes more important, and $(\delta^d_{23})_{LL}$ is strongly constrained by $B \to X_s\gamma$ and $B_s$ mixing constraints. The results are shown in Fig. 3. The allowed region of $(\delta^d_{23})_{LL}$ is the narrow unhatched blue strip in Fig. 3(a). Comparing Figs. 2(b) and 3(b), one also finds that the phase of $B_s$–$\bar{B}_s$ mixing is more tightly constrained compared to the previous case with $\tan\beta = 3$. Also, $S^{\phi K}_{CP}$ and $A^{b\to s\gamma}_{CP}$ can deviate from their SM values significantly through the induced $LR$ insertion. Figure 3(a) reveals that the narrow strip allowed by $B_s$ mixing and $B \to X_s\gamma$ leads to $S^{\phi K}_{CP}$ out of its $2\sigma$ range. In this sense, this case with large $LL$ insertion and moderately high $\tan\beta$ is disfavored by the current $B$ physics data. The predicted range of $S^{\phi K}_{CP}$ is found to be higher than its SM value, around 0.9, in Fig. 3(c). In Fig. 3(d), we find that the blue unhatched region corresponds to $A^{b\to s\gamma}_{CP}$ around negative several percent.

### B. *RR* insertion case

Next, we consider the $RR$ insertion case for $\tan\beta = 3, 10$, which are shown in Figs. 4 and 5. The shapes of the allowed regions, after the $B \to X_s\gamma$ constraint is imposed, are different from those in the $LL$ insertion case, since there is no interference between the SUSY amplitude (the original $RR$ or the induced $RL$ type) and the SM amplitude ($LR$ type). However, the general tendency is similar to the $LL$ insertion case: namely, the induced $RL$

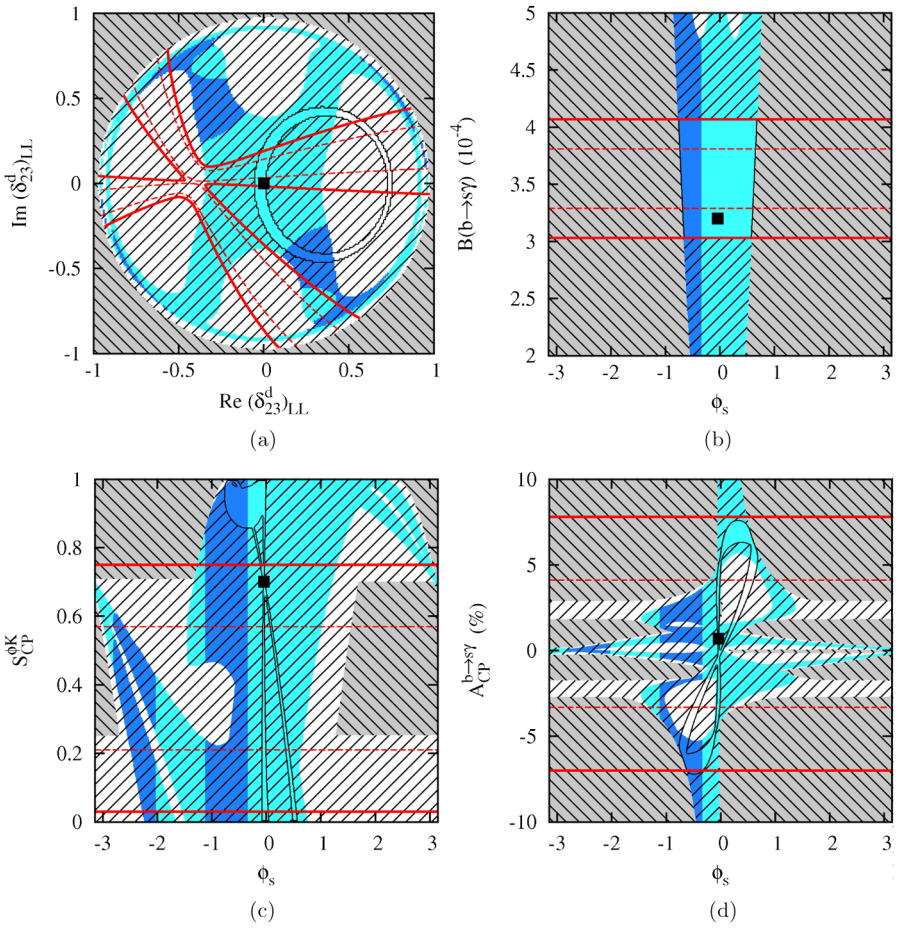


FIG. 3 (color online). Plots with the $LL$ insertion for $\tan\beta = 10$. The meaning of each region is the same as in Fig. 2.

insertion involving the double mass insertion is constrained by the $B \to X_s\gamma$ branching ratio, and the constraint becomes severer for larger $\tan\beta$.

In Fig. 4(a), the $\Delta M_s$ and $\phi_s$ constraints again exclude the origin and require nonzero squark mixing depicted by the blue region. We observe that $B \to X_s\gamma$ leaves a broader region than in the $LL$ case [compare Figs. 4(a) and 2(a)]. In particular, there remains a larger portion of unhatched blue region, due to the weaker constraint from $B \to X_s\gamma$. Still, only one of the two solutions of $\phi_s$ is allowed in Fig. 4(b). The induced $RL$ insertion can lead to sizable changes in $S^{\phi K}_{CP}$ and/or $S^{K^*\gamma}_{CP}$ as well, as shown in Figs. 4(c) and 4(d). Each of them deviates from its SM value due to the $O(1)$ phase of $(\delta^d_{23})_{RR}$ favored by $\phi_s$, under the $B \to X_s\gamma$ constraint. Although $S^{\phi K}_{CP}$ is expelled from the SM point, it can still remain consistent with its measurements. Note that $S^{K^*\gamma}_{CP}$ could be as large as around $\pm 0.8$, and these values are in fact preferred by $\phi_s$ and $B \to X_s\gamma$. This would be clearly tested at $B$ factories.

For $\tan\beta = 10$, the double mass insertion becomes more important, and $(\delta^d_{23})_{RR}$ is strongly constrained by both $B \to X_s\gamma$ and $B_s$ mixing. The results are shown in Fig. 5(a). In this case, the region of $(\delta^d_{23})_{RR}$ allowed by $B \to X_s\gamma$ and $\Delta M_s$ is smaller than the previous case with $\tan\beta = 3$. Moreover, the limitation is so strong that the measured value of $\phi_s$ cannot be reached. Therefore, this case with large $RR$ insertion and moderately high $\tan\beta$ is disfavored by the current $B$ physics data. Indeed, $\phi_s$ is confined within a narrow range around the SM value and thus no unhatched blue region can be found in Fig. 5(b). Forgetting about the current status of $\phi_s$, one might estimate effects of the $RR$ insertion within the unhatched cyan region on $S^{\phi K}_{CP}$ and $A^{b\to s\gamma}_{CP}$. They may deviate from their SM values significantly through induced $RL$ insertion, as shown in Figs. 5(c) and 5(d).

### C. $LL = RR$ case

In this section, we consider the $LL = RR$ case with $\tan\beta = 3, 10$, which are shown in Figs. 6 and 7, respectively. In this case, the supersymmetric effect on $B_s$–$\bar{B}_s$ mixing is greatly enhanced compared to the $LL$ or the $RR$ insertion case, while that on $B \to X_s\gamma$ is not. Thus, only a tiny region around zero is allowed even for small $\tan\beta = 3$, shown in Fig. 6(a). The phase of the mixing is not constrained significantly by $B \to X_s\gamma$, and this decay alone allows for an arbitrary $\phi_s$, as can be seen in the other three

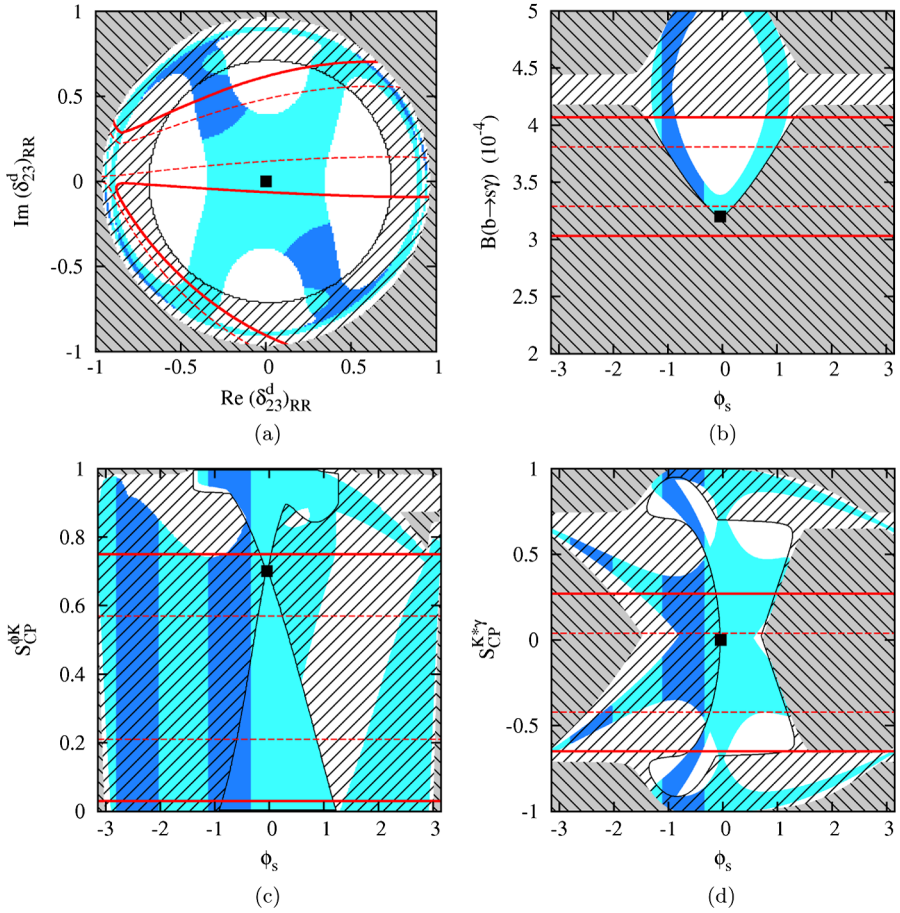


FIG. 4 (color online). The $RR$ insertion case with $\tan\beta = 3$. The meaning of each region is the same as in Fig. 2.

plots. These plots also show variations in $S^{K^*\gamma}_{CP}$, $S^{\phi K}_{CP}$, and $A^{b\to s\gamma}_{CP}$, but they are much smaller than are found in the preceding cases with a single insertion of either chirality, since $\Delta M_s$ allows a much smaller squark mixing. This means that this case can account for the current data of $\phi_s$ as well as $\Delta M_s$ while obeying the other constraints on $CP$ asymmetries under consideration. Still, differences of $S^{K^*\gamma}_{CP}$ and $S^{\phi K}_{CP}$ from their SM predictions can be comparable to or larger than their sensitivities at a super $B$ factory, while $A^{b\to s\gamma}_{CP}$ is not altered enough. Note that the blue region again implies a nonvanishing discrepancy in $S^{\phi K}_{CP}$.

The results for a higher $\tan\beta = 10$ are shown in Fig. 7. The $B \to X_s\gamma$ constraint becomes stronger. Because of this, the range of $\phi_s$ is reduced, but it can still be consistent with the present data. Also, the increased effect of the double insertion leads to larger deviations in $S^{K^*\gamma}_{CP}$, $S^{\phi K}_{CP}$, and $A^{b\to s\gamma}_{CP}$. In particular, one finds that the unhatched blue region leading to $S^{\phi K}_{CP} \sim 0.9$ is excluded from its $2\sigma$ band in Fig. 7(c). Therefore this case is disfavored by the current data. Note that the SUSY effect in $S^{\phi K}_{CP}$ depends on the sum of the $LL$ and $RR$ (or $LR$ and $RL$) insertions, and this makes a clear difference between the predictions of $CP$ asymmetry in this case and the next.

### D. $LL = -RR$ case

In this section, we consider the $LL = -RR$ case. The results for $\tan\beta = 3$ are shown in Fig. 8. Note that the $B_s$–$\bar{B}_s$ mixing constraint is again much stronger than a case with a single insertion of either chirality, and only a tiny region around zero is allowed. The phase of the mixing can be arbitrary even after $B \to X_s\gamma$ has been imposed, as is shown in Fig. 8(b). The deviation in $S^{K^*\gamma}_{CP}$ can be comparable to or larger than its sensitivities at a super $B$ factory, while $A^{b\to s\gamma}_{CP}$ is not altered enough. In this case, $S^{\phi K}_{CP}$ does not move from its SM value, as the SUSY effect in $S^{\phi K}_{CP}$ depends on the sum of the $LL$ and $RR$ (or $LR$ and $RL$) insertions which cancel each other. Therefore $S^{\phi K}_{CP}$ is not affected even for higher $\tan\beta$. Instead, $S^{\eta' K}_{CP}$ should show a discrepancy as it depends on the difference of the $LL$ and $RR$ (or $LR$ and $RL$) insertions.

Results for a higher $\tan\beta = 10$ are shown in Fig. 9. The $B \to X_s\gamma$ constraint becomes stronger. Nevertheless, $\phi_s$ is allowed to have an arbitrary value. Deviations in $S^{K^*\gamma}_{CP}$ and $A^{b\to s\gamma}_{CP}$ have been amplified relative to the previous case with $\tan\beta = 3$. As was mentioned above, $S^{\phi K}_{CP}$ remains at its SM prediction. This helps the present case to be compatible with all of the experimental inputs, $B \to X_s\gamma$, $\Delta M_s$,

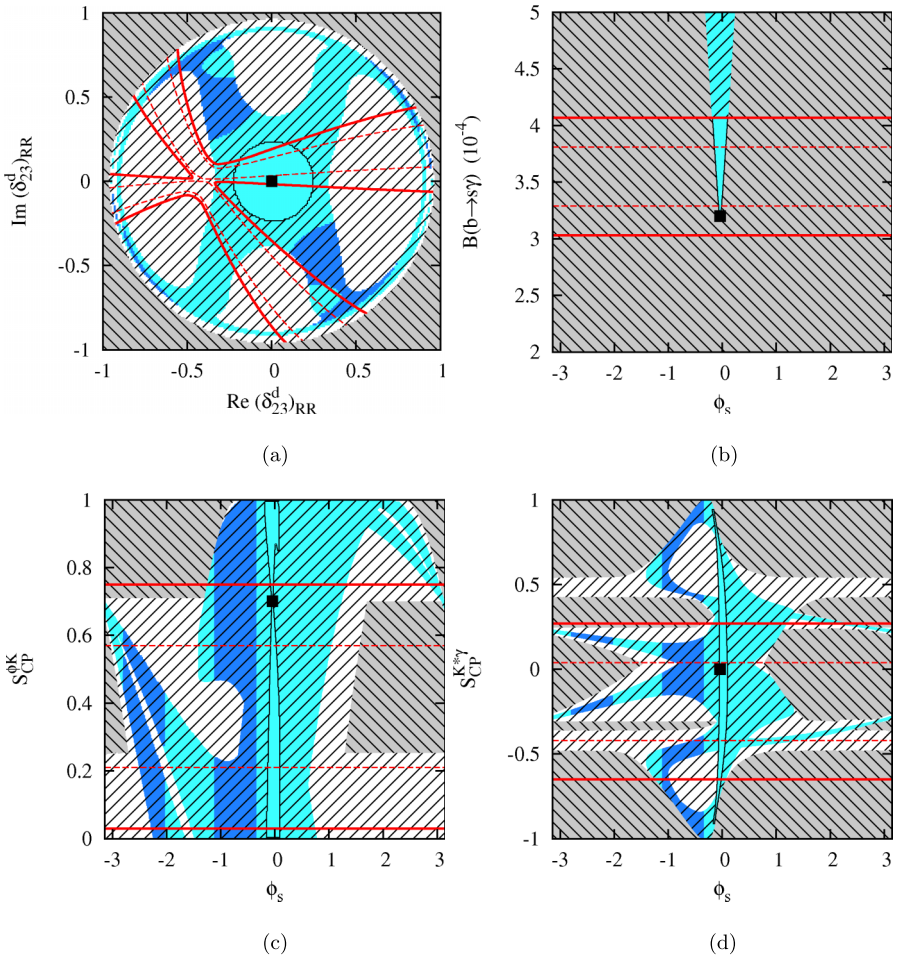


FIG. 5 (color online). Plots with the $RR$ insertion for $\tan\beta = 10$. The meaning of each region is the same as in Fig. 2.

$\phi_s$, and $S^{\phi K}_{CP}$, even for a moderately high $\tan\beta$. Recall that the $LL = RR$ case, by contrast, was in conflict with $S^{\phi K}_{CP}$ for the same value of $\tan\beta$. The phase of mass insertions in the unhatched blue region causes nonvanishing deviations in $S^{K^*\gamma}_{CP}$ and $A^{b\to s\gamma}_{CP}$, to such an extent that can be tested at a $B$ factory.

## IV. IMPLICATIONS FOR SUSY MODELS

In Sec. III, we derived the constraint on $(\delta^d_{23})_{LL}$ and $(\delta^d_{23})_{RR}$. The size of each $\delta$ is determined by theories for the soft SUSY breaking, or SUSY breaking mediation mechanisms. There are basically three categories in the solutions to the SUSY flavor and $CP$ problems:

(i) universal scalar masses at some messenger scale
(ii) alignment of quark and squark mass matrices in the flavor space using some flavor symmetry
(iii) decoupling (effective SUSY scenario).

In this section, we discuss implications of the analysis in the previous section on the flavor structures of the soft terms at high energy scale and on SUSY flavor models, for the first two categories listed above to which our results are applicable.

### A. SUSY models with universal scalar masses

Let us first discuss the flavor physics within SUSY scenarios where one has universal soft terms at some high energy messenger scale $M_{\rm mess}$. In this case, the SUSY flavor problem is solved by assuming universal squark mass matrices at $M_{\rm mess}$. Nonetheless at electroweak scale, nonvanishing mass insertion parameters are generated by RG evolution, which is calculable in terms of the Yukawa couplings. Namely, $\delta_{ij}(M_{\rm mess}) = 0$, and nonzero $\delta$'s at the electroweak scale are generated by RG evolutions. Models belonging to this category include the so-called minimal supergravity (mSUGRA) or gauge mediation SUSY breaking scenarios, dilaton dominated SUSY breaking within superstring models.

For example, within mSUGRA, one has [42]

$$(\Delta_{ij})_{LL}(M_Z) \simeq -\frac{1}{8\pi^2} Y_t^2 (V_{\rm CKM})_{3i}(V^*_{\rm CKM})_{3j}(3m_0^2 + a_0^2) \times \log\left(\frac{M_*}{M_Z}\right), \tag{4.1}$$

so that $(\delta^d_{LL})_{23} \simeq 10^{-2}$ and $(\delta_{LL})_{13} \simeq 8 \times 10^{-3} \times e^{-i2.7}$. This size of $(\delta^d_{23})_{LL}$ might be regarded as being perfectly

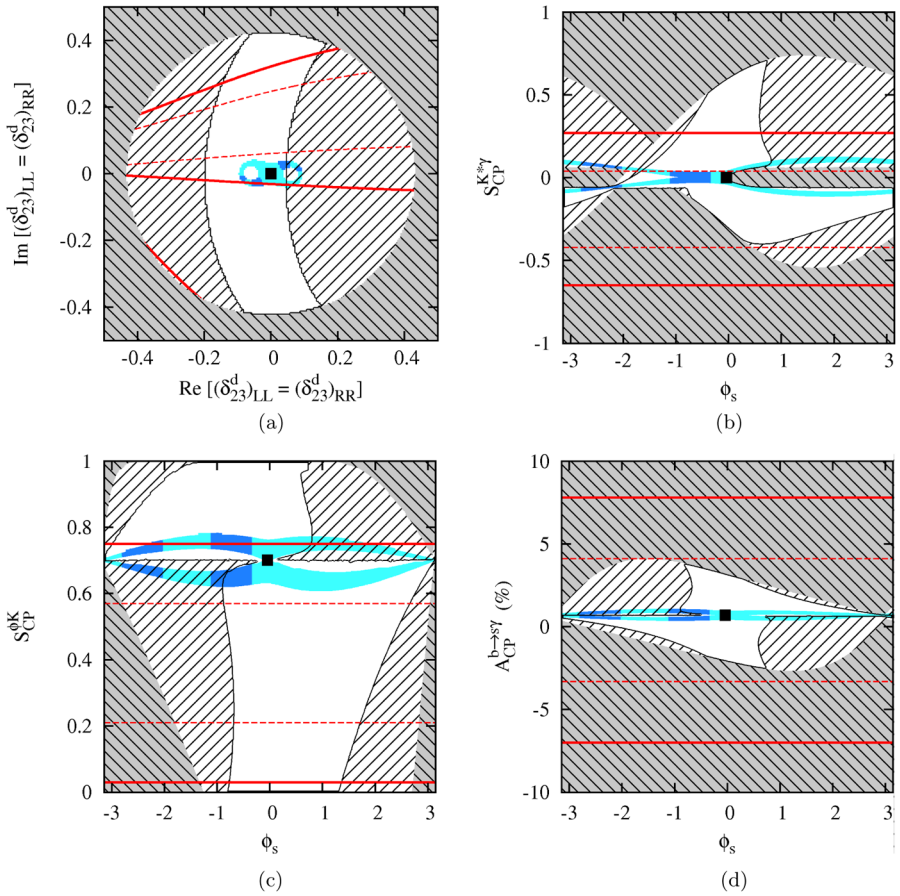


FIG. 6 (color online). Plots for the $LL = RR$ case with $\tan\beta = 3$. The meaning of each region is the same as in Fig. 2.

fine with the constraints we discussed in Sec. III A, unless one cares about the current status of $\phi_s$. If one is interested in fitting the present data of $\phi_s$, this scenario is not a good choice. In particular, the phase of $(\delta^d_{23})_{LL}$ is $-0.02$. Therefore, there would be only small deviations in $\phi_s$, $S^{\phi K}_{CP}$, or $A^{b\to s\gamma}_{CP}$ within this scenario. There could be some effects in $b \to d$ transition, including $B \to X_d\gamma$, and we refer to Ref. [19] for further details.

If we consider a SUSY grand unified theory (GUT) with right-handed neutrinos, the situation can change, however. In many SUSY GUT models, the left-handed lepton doublet sits in the same representation as the left-handed anti-down-quark triplets. Then, the large mixing in the atmospheric neutrinos could be related with the large mixing in the $\tilde{b}_R$-$\tilde{s}_R$ sector [23,43,44], unless the main source of neutrino mixings is the Majorana right-handed neutrino mass terms. Therefore there could be large $b \to s$ transitions in the low energy processes in such scenarios, and $B_s$ mixing or $B_d \to \phi K_S$ $CP$ asymmetries can differ significantly from the SM predictions.

For example, in SU(5) with right-handed neutrinos, one has [23,43]

$$(m^2_{\tilde{d}})_{ij} \simeq -\frac{1}{8\pi^2}[Y^\dagger_N Y_N]_{ij}(3m_0^2 + A^2)\log\frac{M_*}{M_{\rm GUT}}$$
$$\simeq -e^{-i(\phi^{(L)}_i - \phi^{(L)}_j)}\frac{y^2_{\nu_k}}{8\pi^2}[V^*_L]_{ki}[V_L]_{kj}(3m_0^2 + A^2)$$
$$\times \log\frac{M_*}{M_{\rm GUT}}.$$

In this scenario, $|(\delta^d_{RR})_{23}| \simeq 2 \times 10^{-2} \times (M_{N_3}/10^{14}\ {\rm GeV})$ with $O(1)$ phase, which is in sharp contrast with the $LL$ insertion, Eq. (4.1). This RG induced $\delta$ alone is small enough to evade the constraint from $\Delta M_s$, but not big enough to accommodate $\phi_s$. On the other hand, the $RR$ insertion is large enough to induce an effective $RL$ insertion of $\sim 10^{-2}$ through the double mass insertion mechanism, and can affect $S^{\phi K}_{CP}$ and $S^{K^*\gamma}_{CP}$. Also in this scenario, there are RG induced $LL$ insertions mentioned above. Combining these two types of insertions, one could get enough effect in $B_s$–$\bar{B}_s$ mixing to fit the current world average of $\phi_s$. However, an obstacle to this purpose is the hadronic electric dipole moment [45]. In particular, it is not easy to circumvent this constraint if one assumes that

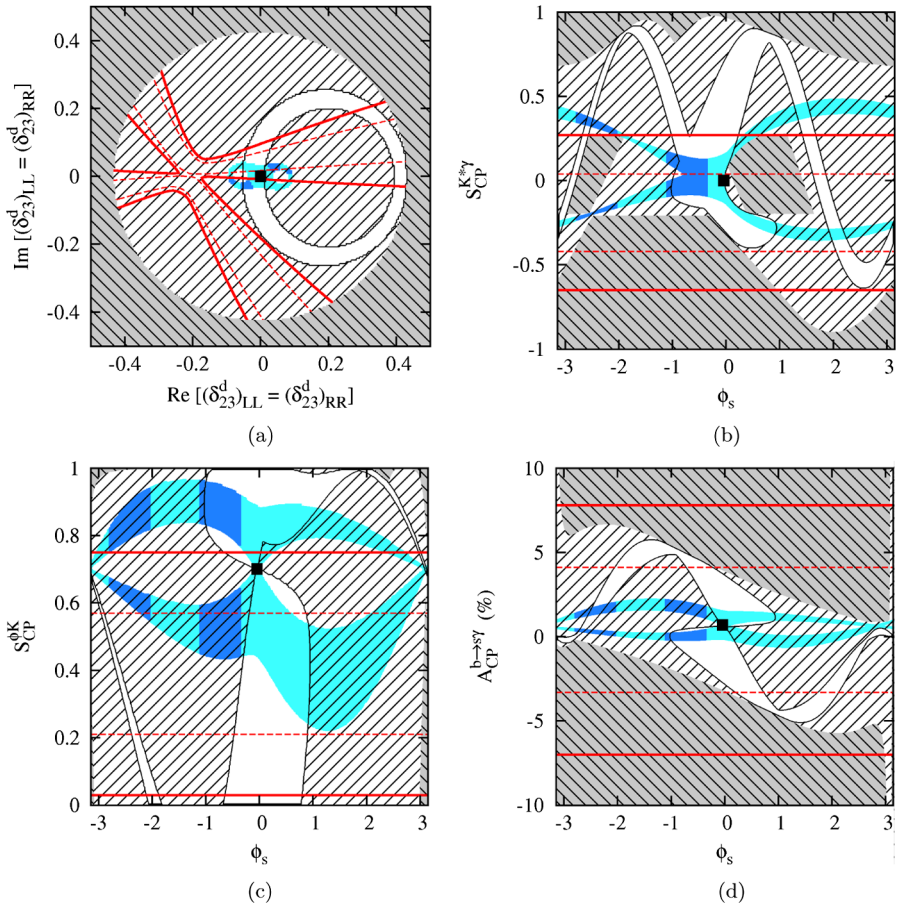


FIG. 7 (color online). Plots for the $LL = RR$ case with $\tan\beta = 10$. The meaning of each region is the same as in Fig. 2.

the $LL$ insertion arises solely from RG evolution, as is the case in this subsection. One of the few ways might be to assume that the first and the second terms in $A_b - \mu\tan\beta$ cancel each other resulting in a small sum, since the supersymmetric contribution to hadronic electric dipole moment is proportional to the sum.

### B. SUSY flavor models

Another way out of the SUSY flavor problem is to invoke some flavor symmetry and make quark and squark mass matrices almost aligned. Alignment of quark and squark mass matrices can be achieved by assuming some flavor symmetries $[U(1), S_3, \ldots]$. We discuss what implications the present analysis may have on those supersymmetric flavor models. We borrow the list of models from Ref. [46], discarding two decoupling-type models therein.

Suppose that a given flavor symmetry is broken around the GUT scale. Then RG evolution of the squark mass matrix down to the weak scale should be taken into account. The diagonal components increase receiving the gluino mass contribution:

$$m^2_{\tilde{q}}(M_Z) \approx m_0^2 + 6M^2_{1/2}, \tag{4.2}$$

where $m_0$ and $M_{1/2}$ are the diagonal squark mass and the gluino mass at the GUT scale. An off-diagonal element does not change very much except for the CKM suppressed contribution in Eq. (4.1). In many cases, a flavor symmetry predicts the ratio of an off-diagonal element to the diagonal one, $(\Delta_{ij})_{AB}/m_0^2$, thereby determining the degree of squark nonuniversality at the scale where it is broken. In terms of this ratio, the mass insertion at weak scale can be written as

$$(\delta^d_{ij})_{AB} \approx \frac{(\Delta_{ij})_{AB}/m_0^2}{1 + 6M^2_{1/2}/m_0^2}, \tag{4.3}$$

using Eq. (4.2). One can notice that the nonuniversality at the GUT scale is diluted in the course of running, depending on the ratio $M^2_{1/2}/m_0^2$. In what follows, we ignore this effect. If one takes it into account, constraints on a model may be eased especially for large $M_{1/2}$. On the other hand, this could also make it more difficult to account for the present $O(1)$ value of $\phi_s$ by reducing the expected size of a mass insertion below what is needed.

The result is shown in Table I. The current status of each model is indicated in the two columns on the right. One can see that availability of the new data on $B_s$–$\bar{B}_s$ mixing enables us to discriminate models according to their predictions on 2–3 mixing of down-type squarks. A model is

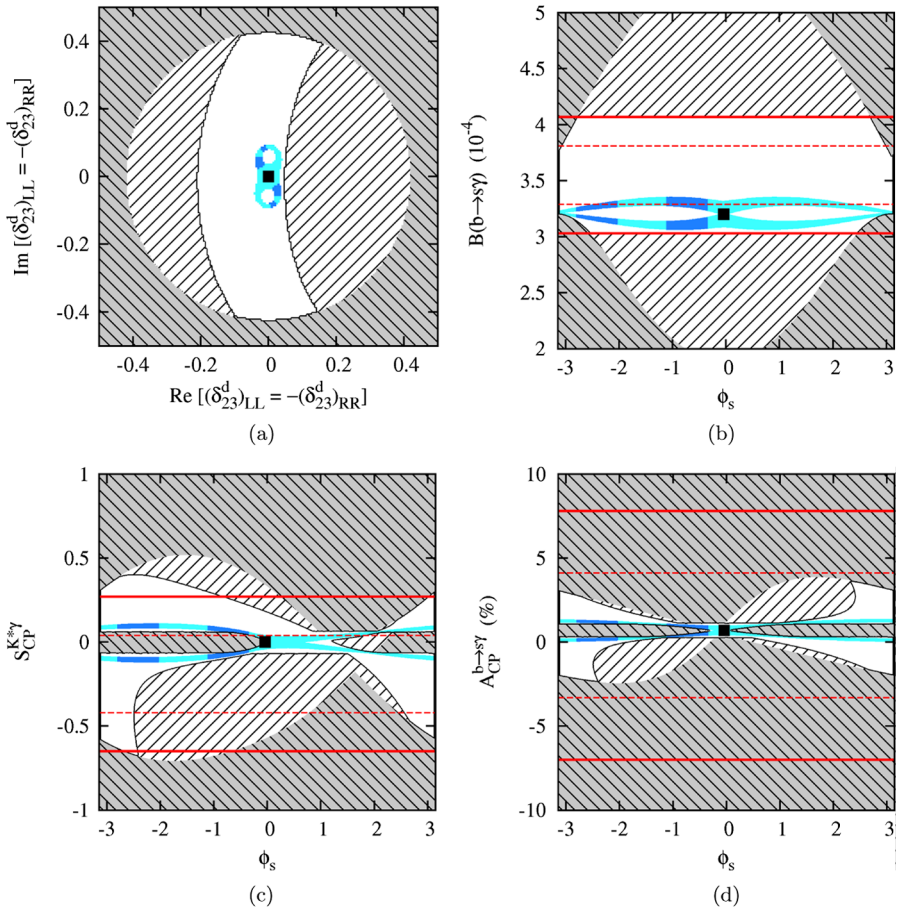


FIG. 8 (color online). Plots for the $LL = -RR$ case with $\tan\beta = 3$. The meaning of each region is the same as in Fig. 2.

marked as being safe if it suppresses flavor violation to such an extent that no appreciable deviation from the SM can be observed. However, such a model may not produce enough difference in $\phi_s$ to account for its current world average. We indicate a class of models that can fit $\phi_s$ while keeping compatibility with the other constraints. They lead to nonzero mass insertions of both chiralities enhancing supersymmetric contribution to $B_s$ mixing. A caveat is dilution of mass insertions mentioned above. Some models leading to sizable mass insertions are about to be in contact with the present experiments or strongly disfavored by them depending on the choice of parameters. A future experiment should be able to resolve this issue and to scrutinize more models. Needless to say, all the above discussions are based on our choice of sparticle mass scale. That is, supersymmetric flavor/$CP$ problems can be mitigated by making sparticles heavier.

Although not directly related to $B_s$–$\bar{B}_s$ mixing, a remark is in order regarding the $D$–$\bar{D}$ mixing constraint. Recently, evidence for $D$–$\bar{D}$ mixing has been reported [55], and this provides restrictions on the up-type mass insertions $(\delta^u_{12})_{AB}$ [56,57]. Since the above models were built before $D$–$\bar{D}$ mixing was measured, not all of them were intended to suppress $(\delta^u_{12})_{AB}$ enough to obey the present upper bounds thereon. Indeed, models in Refs. [47,48,50] and the Abelian model in Ref. [49] (labeled as [49]a in Table I) likely imply $(\delta^u_{12})_{LL} \sim \lambda$. This is a generic feature of an Abelian alignment model, stemming from Cabibbo mixing and nondegeneracy of diagonal squark mass components [47,48]. Given the 95% probability upper bound $(\delta^u_{12})_{LL} < 0.049$ for squark and gluino masses of 500 GeV [56], Abelian alignment models are strongly disfavored. Non-Abelian models are better in this respect, and most of those in the table are safe. One model that predicts a rather sizable effect on $D$–$\bar{D}$ mixing is that in Ref. [54]. It predicts $\sqrt{(\delta^u_{12})_{LL}(\delta^u_{12})_{RR}} \sim \lambda^{3.5} \sim 0.005$. The 95% probability upper bound on this geometric average of mass insertions is 0.0029 for squark and gluino masses of 500 GeV [56]. As in $B$ mixing, supersymmetric effects on $D$–$\bar{D}$ mixing are enhanced if both $LL$ and $RR$ insertions are nonzero. Therefore, this model is on the verge of experimental probe.

## V. CONCLUSIONS

In conclusions, we studied the implication of the recent measurements of $B_s$–$\bar{B}_s$ mixing on the mass insertion parameters in the general SUSY models and on the

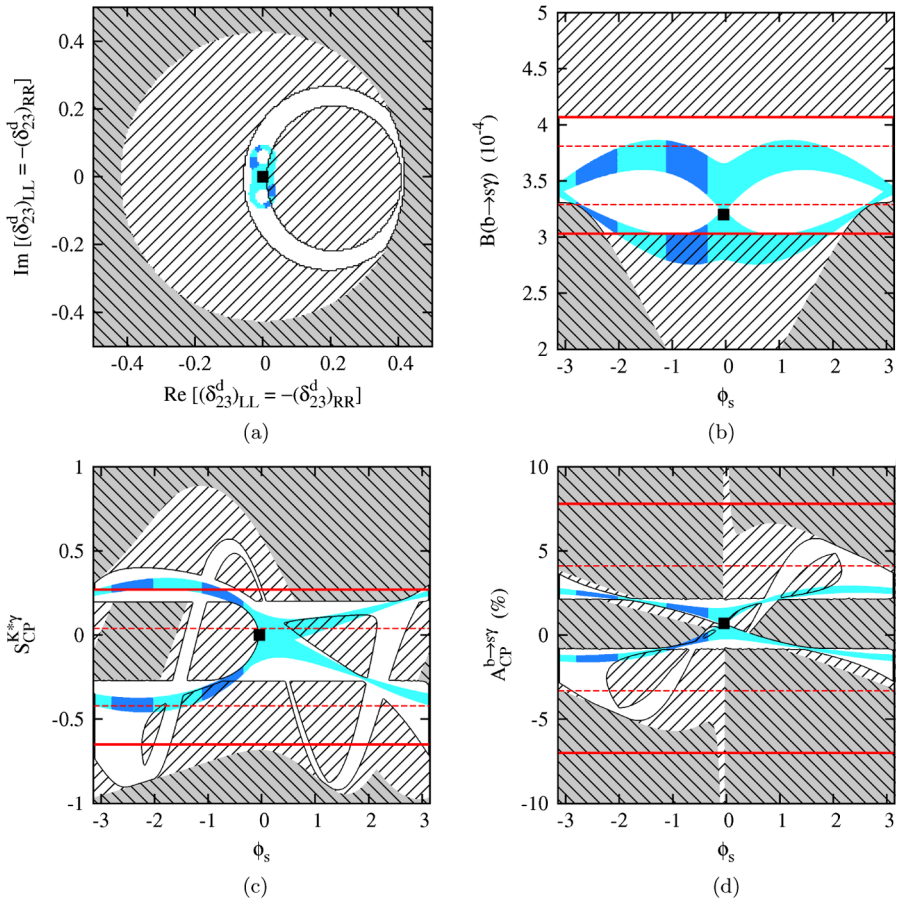


FIG. 9 (color online). Plots for the $LL = -RR$ case with $\tan\beta = 10$. The meaning of each region is the same as in Fig. 2

SUSY flavor models. The recent measurements of $\Delta M_s$ constrains the CKM element $|V_{td}|$, which is consistent with the Belle result extracted from $b \to d\gamma$. This constitutes another test of the CKM paradigm of the SM for flavor and $CP$ violation in the quark sector. The measurement of $\Delta M_s$ begins to put strong constraint on new physics scenarios, and a room for the new physics contribution to $b \to s$ transition is getting tight now, and will be even more so in the future. Even the very first data on $\Delta M_s$ from D0 and CDF already constrain either of the $LL$ and the $RR$ insertions, which should be compared with the bounds $\lesssim O(1)$ in [17] or [26]. For the $LL = \pm RR$ case, the constraints are even stronger, and the allowed mass insertion parameters are tiny even for small $\tan\beta = 3$. Still there could be moderate to large deviations in $A_{CP}^{b\to s\gamma}$, $S_{CP}^{K^*\gamma}$, or $S_{CP}^{\phi K}$ through the double mass insertion effects for the large $\tan\beta$ case. It is imperative to measure these observables, and confirm the SM predictions on these observables both at hadron colliders and at (super) $B$ factories, in order to test the CKM paradigm in the $b \to s$ transition.

TABLE I. Status of part of the models analyzed in Ref. [46], for the two different values of $\tan\beta$. Each case is classified into one of the following four categories: ( · ) incompatible with $\phi_s$ but safe otherwise; ($\phi_s$) compatible with $\phi_s$ and safe; ($\surd$) currently okay but dangerous; ($\times$) disfavored.

| Model | $\lvert(\delta^d_{23})_{LL}\rvert$ | $\lvert(\delta^d_{23})_{RR}\rvert$ | $\tan\beta = 3$ | $\tan\beta = 10$ |
|---|---|---|---|---|
| [47] | $\lambda^2$ | $\lambda^4$ | · | $\surd$ |
| [48], [49]a | $\lambda^2$ | 1 | $\times$ | $\times$ |
| [50] | $\lambda^2$ | $\lambda^8$ | · | $\surd$ |
| [49]b | $\lambda^2$ | $\lambda^{1/2}$ | $\times$ | $\times$ |
| [51], [52]b | $\lambda^2$ | $\lambda^2$ | $\phi_s$ | $\surd$ |
| [53] | $\lambda^3$ | $\lambda^5$ | · | · |
| [54] | $\lambda^2$ | $\lambda^4$ | · | $\surd$ |

In a model independent approach, one can say that $CP$ violation in $B_s \to J/\psi\phi$ and $A_{\rm SL}$ give additional information on the phase of $B_s$–$\bar{B}_s$ mixing, and can make a firm test of the CKM paradigm in the SM, and constrain various new physics scenarios. $CP$ asymmetries in $B \to \phi K_S$, $\eta' K_S$, $K_S\pi^0, \ldots$ can differ from the SM predictions to some extent, but we cannot make definite predictions within the model independent approach.

Within general SUSY models with gluino-mediated $b \to s$ transition, one can summarize the implications of the $\Delta M_s$ and $\phi_s$ measurements as follows:

(i) The $LL$ or $RR$ insertions for the small $\tan\beta$ case cannot be large as in the past ( $\lesssim 0.5$).

(ii) The large tan$\beta$ case is strongly constrained by $b \to s\gamma$.
(iii) The $LL = \pm RR$ case is even more strongly constrained by $\Delta M_s$ measurement.
(iv) The $LR$ or $RL$ insertions consistent with $b \to s\gamma$ is still fine with $\Delta M_s$, since it does not affect $B_s$–$\bar{B}_s$ mixing; however for the same reason, it cannot make an $O(1)$ difference in $\phi_s$.
(v) Definite relations between $\Delta B = 2$ and $\Delta B = 1$ processes $CP$ asymmetries in $B \to \phi K_S$, $\eta' K_S$, $K_S\pi^0, \ldots$ can differ from the SM predictions to some extent, and we can make definite predictions within SUSY models (modulo hadronic uncertainties).
(vi) $B_d \to \phi K_S$ can still differ from the SM prediction, if the (induced) $LR$ or $RL$ insertions are present at the level of $10^{-2}$–$10^{-3}$.

Whether the present hint of new physics in the $B_s$ mixing phase will persist in the future or not will be an interesting topic within the coming years for $B$ factories and hadron colliders, and the data will show whether the SM explains $b \to s$ transition perfectly, or some new physics is in need. In particular, it is important to improve the precision of time-dependent $CP$ asymmetries in $B_s \to J/\psi\phi$ and $B_d \to \phi K_S$, and the direct $CP$ asymmetry in $B \to X_s\gamma$ etc., and confront the measured data with the SM predictions, in order to confirm the Kobayashi-Maskawa paradigm or discover indirect new physics effects.

## ACKNOWLEDGMENTS

We are grateful to Intae Yu for discussions on the experimental data from D0 and CDF. P. K. is supported in part by KOSEF through the SRC program at CHEP, Kyungpook National University. J.-h. P. acknowledges Research Grants funded jointly by the Italian Ministero dell'Istruzione, dell'Università e della Ricerca (MIUR), by the University of Padova and by the Istituto Nazionale di Fisica Nucleare (INFN) within the *Astroparticle Physics Project* and the FA51 INFN Research Project. He was also supported in part by the European Community Research Training Network UniverseNet under Contract No. MRTN-CT-2006-035863.

[1] N. Cabibbo, Phys. Rev. Lett. **10**, 531 (1963); M. Kobayashi and T. Maskawa, Prog. Theor. Phys. **49**, 652 (1973).
[2] V. M. Abazov *et al.* (D0 Collaboration), Phys. Rev. Lett. **97**, 021802 (2006).
[3] A. Abulencia *et al.* (CDF Collaboration), Phys. Rev. Lett. **97**, 242003 (2006).
[4] K. Abe *et al.*, Phys. Rev. Lett. **96**, 221601 (2006).
[5] J. Charles *et al.* (CKMfitter Group), Eur. Phys. J. C **41**, 1 (2005), updated results and plots available at http://ckmfitter.in2p3.fr/.
[6] E. Barberio *et al.*, arXiv:0808.1297.
[7] Y. Grossman, Y. Nir, and G. Raz, Phys. Rev. Lett. **97**, 151801 (2006).
[8] A. Lenz and U. Nierste, J. High Energy Phys. 06 (2007) 072.
[9] M. Ciuchini and L. Silvestrini, Phys. Rev. Lett. **97**, 021803 (2006); M. Endo and S. Mishima, Phys. Lett. B **640**, 205 (2006); P. Ball and R. Fleischer, Eur. Phys. J. C **48**, 413 (2006); S. Khalil, Phys. Rev. D **74**, 035005 (2006); S. Baek, J. High Energy Phys. 09 (2006) 077; R. Arnowitt, B. Dutta, B. Hu, and S. Oh, Phys. Lett. B **641**, 305 (2006); B. Dutta and Y. Mimura, Phys. Rev. Lett. **97**, 241802 (2006); X. Ji, Y. Li, and Y. Zhang, Phys. Rev. D **75**, 055016 (2007).
[10] J. Foster, K. i. Okumura, and L. Roszkowski, Phys. Lett. B **641**, 452 (2006).
[11] A. Datta, Phys. Rev. D **74**, 014022 (2006); X. G. He and G. Valencia, Phys. Rev. D **74**, 013011 (2006); M. Blanke, A. J. Buras, A. Poschenrieder, C. Tarantino, S. Uhlig, and A. Weiler, J. High Energy Phys. 12 (2006) 003; C. W. Chiang, N. G. Deshpande, and J. Jiang, J. High Energy Phys. 08 (2006) 075; S. Baek, J. H. Jeon, and C. S. Kim, Phys. Lett. B **641**, 183 (2006); A. J. Buras, A. Poschenrieder, S. Uhlig, and W. A. Bardeen, J. High Energy Phys. 11 (2006) 062; S. Chang, C. S. Kim, and J. Song, J. High Energy Phys. 02 (2007) 087; L. x. Lu and Z. j. Xiao, Commun. Theor. Phys. **47**, 1099 (2007); A. Dighe, A. Kundu, and S. Nandi, Phys. Rev. D **76**, 054005 (2007); R. Mohanta and A. K. Giri, Phys. Rev. D **76**, 075015 (2007); A. Lenz, Phys. Rev. D **76**, 065006 (2007); S. L. Chen, X. G. He, X. Q. Li, H. C. Tsai, and Z. T. Wei, Eur. Phys. J. C **59**, 899 (2009); J. P. Lee and K. Y. Lee, Phys. Rev. D **78**, 056004 (2008).
[12] For a review, see e.g. Y. Nir, arXiv:hep-ph/0510413.
[13] For a review, see e.g. R. Fleischer, arXiv:0802.2882.
[14] V. M. Abazov *et al.* (D0 Collaboration), Phys. Rev. Lett. **101**, 241801 (2008).
[15] T. Aaltonen *et al.* (CDF Collaboration), Phys. Rev. Lett. **100**, 161802 (2008).
[16] G. L. Kane, P. Ko, H. b. Wang, C. Kolda, J.-h. Park, and L. T. Wang, Phys. Rev. Lett. **90**, 141803 (2003).
[17] G. L. Kane, P. Ko, H. b. Wang, C. Kolda, J.-h. Park, and L. T. Wang, Phys. Rev. D **70**, 035015 (2004).
[18] For a review, see e.g. S. P. Martin, arXiv:hep-ph/9709356.
[19] P. Ko, J.-h. Park, and G. Kramer, Eur. Phys. J. C **25**, 615 (2002).
[20] L. J. Hall, V. A. Kostelecky, and S. Raby, Nucl. Phys. **B267**, 415 (1986).
[21] S. Baek, D. G. Cerdeno, Y. G. Kim, P. Ko, and C. Munoz, J. High Energy Phys. 06 (2005) 017.
[22] D. Becirevic *et al.*, Nucl. Phys. **B634**, 105 (2002).

[23] T. Moroi, Phys. Lett. B **493**, 366 (2000).
[24] M. Okamoto, Proc. Sci., LAT2005 (2006) 013 [arXiv:hep-lat/0510113].
[25] F. Borzumati, C. Greub, T. Hurth, and D. Wyler, Phys. Rev. D **62**, 075005 (2000).
[26] M. Ciuchini, E. Franco, A. Masiero, and L. Silvestrini, Phys. Rev. D **67**, 075016 (2003); **68**, 079901(E) (2003).
[27] F. Gabbiani and A. Masiero, Nucl. Phys. **B322**, 235 (1989).
[28] S. Baek, J. H. Jang, P. Ko, and J.-h. Park, Phys. Rev. D **62**, 117701 (2000); Nucl. Phys. **B609**, 442 (2001).
[29] R. Harnik, D. T. Larson, H. Murayama, and A. Pierce, Phys. Rev. D **69**, 094024 (2004); M. Endo, S. Mishima, and M. Yamaguchi, Phys. Lett. B **609**, 95 (2005).
[30] M. Ciuchini and L. Silvestrini, Phys. Rev. Lett. **97**, 021803 (2006).
[31] M. Endo and S. Mishima, Phys. Lett. B **640**, 205 (2006).
[32] K. i. Okumura and L. Roszkowski, Phys. Rev. Lett. **92**, 161801 (2004); J. High Energy Phys. 10 (2003) 024.
[33] J. Hisano and Y. Shimizu, Phys. Rev. D **70**, 093001 (2004); J. Hisano, M. Kakizaki, M. Nagai, and Y. Shimizu, Phys. Lett. B **604**, 216 (2004).
[34] V. M. Abazov *et al.* (D0 Collaboration), Phys. Rev. Lett. **98**, 151801 (2007); **98**, 121801 (2007); Phys. Rev. D **76**, 057101 (2007).
[35] M. Bona *et al.* (UTfit Collaboration), arXiv:0803.0659.
[36] D. Atwood, M. Gronau, and A. Soni, Phys. Rev. Lett. **79**, 185 (1997).
[37] A. Dedes and A. Pilaftsis, Phys. Rev. D **67**, 015012 (2003); M. S. Carena, A. Menon, R. Noriega-Papaqui, A. Szynkman, and C. E. M. Wagner, Phys. Rev. D **74**, 015009 (2006); M. Blanke, A. J. Buras, D. Guadagnoli, and C. Tarantino, J. High Energy Phys. 10 (2006) 003; G. Isidori and P. Paradisi, Phys. Lett. B **639**, 499 (2006).
[38] A. Lenz and U. Nierste, J. High Energy Phys. 06 (2007) 072.
[39] V. M. Abazov *et al.* (D0 Collaboration), Phys. Rev. D **76**, 057101 (2007).
[40] I. Dunietz, R. Fleischer, and U. Nierste, Phys. Rev. D **63**, 114015 (2001).
[41] M. Beneke, G. Buchalla, M. Neubert, and C. T. Sachrajda, Phys. Rev. Lett. **83**, 1914 (1999); Nucl. Phys. **B591**, 313 (2000); **B606**, 245 (2001).
[42] L. Alvarez-Gaume, M. Claudson, and M. B. Wise, Nucl. Phys. **B207**, 96 (1982).
[43] T. Moroi, J. High Energy Phys. 03 (2000) 019.
[44] D. Chang, A. Masiero, and H. Murayama, Phys. Rev. D **67**, 075013 (2003).
[45] Pyungwon Ko, Jae-hyeon Park, and Masahiro Yamaguchi, J. High Energy Phys. 11 (2008) 051.
[46] L. Randall and S. f. Su, Nucl. Phys. **B540**, 37 (1999).
[47] M. Leurer, Y. Nir, and N. Seiberg, Nucl. Phys. **B420**, 468 (1994).
[48] Y. Nir and N. Seiberg, Phys. Lett. B **309**, 337 (1993).
[49] C. D. Carone, L. J. Hall, and T. Moroi, Phys. Rev. D **56**, 7183 (1997).
[50] Y. Nir and R. Rattazzi, Phys. Lett. B **382**, 363 (1996).
[51] R. Barbieri, L. J. Hall, S. Raby, and A. Romanino, Nucl. Phys. **B493**, 3 (1997).
[52] A. Pomarol and D. Tommasini, Nucl. Phys. **B466**, 3 (1996).
[53] L. J. Hall and H. Murayama, Phys. Rev. Lett. **75**, 3985 (1995); C. D. Carone, L. J. Hall, and H. Murayama, Phys. Rev. D **53**, 6282 (1996).
[54] P. Pouliot and N. Seiberg, Phys. Lett. B **318**, 169 (1993).
[55] B. Aubert *et al.* (*BABAR* Collaboration), Phys. Rev. Lett. **98**, 211802 (2007); M. Staric *et al.* (Belle Collaboration), Phys. Rev. Lett. **98**, 211803 (2007); L. M. Zhang *et al.* (Belle Collaboration), Phys. Rev. Lett. **99**, 131803 (2007).
[56] M. Ciuchini, E. Franco, D. Guadagnoli, V. Lubicz, M. Pierini, V. Porretti, and L. Silvestrini, Phys. Lett. B **655**, 162 (2007).
[57] Y. Nir, J. High Energy Phys. 05 (2007) 102.